© 2026 | EISSN: 3141-2343|

# PHYTOCHEMICALLY MEDIATED FABRICATION OF NICKEL OXIDE NANOPARTICLE/CARBON DOT COMPOSITES: STRUCTURAL CHARACTERIZATION AND ENHANCED ANTIMICROBIAL EFFICACY

Habtamu Fekadu Etefa[1,2]

[1]*Material Science Unit, National Taiwan University of Science and Technology, Taiwan*
[2]*Department of Physics, Dambi Dollo University, Ethiopia*

Corresponding Author: dr.habtamu@dadu.edu.et

## Abstract

The escalating prevalence of antimicrobial resistance has created an urgent demand for novel, ecologically responsible antibacterial and antifungal agents. This study reports the phytochemically mediated green synthesis of nickel oxide nanoparticles (NiO NPs) using Croton macrostachyus leaf extract and their subsequent hybridization with carbon dots (C-dots) to produce NiO NPs@C-dot composites with enhanced antimicrobial properties. The NiO NPs were synthesized by combining Croton macrostachyus leaf extract with nickel nitrate hexahydrate, followed by calcination at 450 °C for 4 hours, while C-dots were separately prepared from citric acid and o-phenylenediamine via hydrothermal treatment. Structural and morphological characterization was accomplished through transmission electron microscopy (TEM), field emission scanning electron microscopy (FE-SEM), energy dispersive X-ray spectroscopy (EDS), X-ray diffraction (XRD), Fourier transform infrared spectroscopy (FT-IR), UV-visible spectroscopy, and electrochemical impedance spectroscopy (EIS). The average particle sizes of NiO NPs and the NiO NPs@C-dot composite were determined to be 25.34 ± 0.12 nm and 24.95 ± 0.22 nm, respectively. XRD analysis confirmed the face centered cubic crystalline phase of the NiO NPs with diffraction peaks indexed to the (111), (200), (220), (311), and (222) planes. The antimicrobial potential of both bare NiO NPs and the composite was evaluated against Gram positive (Bacillus subtilis and Staphylococcus aureus), Gram negative (Escherichia coli and Pseudomonas aeruginosa) bacterial strains, and the fungal strain Fusarium using the agar well diffusion method. The NiO NPs@C-dot composite exhibited superior antimicrobial activity with zones of inhibition ranging from 22 to 26 mm compared with 21 to 24 mm for bare NiO NPs, attributable to the synergistic enhancement of reactive oxygen species generation and improved surface interactions conferred by the C-dot coating. These findings establish the NiO NPs@C-dot composite as a promising candidate for biomedical antimicrobial applications.

**Keywords:** Nickel oxide nanoparticles; Carbon dots; Green synthesis; Antimicrobial activity; Croton macrostachyus; Nanocomposite; Reactive oxygen species

## 1. Introduction

The rapid proliferation of drug resistant microbial pathogens constitutes one of the most formidable public health challenges of the twenty first century. Conventional antibiotics are increasingly failing to combat infections caused by multidrug resistant bacteria, necessitating the exploration of alternative therapeutic strategies (Pokrajac et al., 2022). Within this context, nanomaterials have emerged as compelling candidates for next generation antimicrobial agents owing to their unique size dependent physicochemical properties, which include elevated surface area to volume ratios, enhanced chemical reactivity, and the capacity to generate reactive oxygen species (ROS) that disrupt microbial cellular integrity (Hao et al., 2010; Brigger et al., 2012).

Among the diverse metal oxide nanoparticles that have been investigated for biomedical applications, nickel oxide nanoparticles (NiO NPs) occupy a prominent position due to their broad spectrum antibacterial efficacy, chemical stability, and versatile functionality spanning energy storage, gas sensing, electrochromic devices, and catalysis (Hussein and Mohammed, 2021; Khalil et al., 2017). The synthesis of NiO NPs through conventional chemical and physical routes, including coprecipitation, sol gel processing, hydrothermal methods, and laser ablation, has been well documented in the literature (El-Kemary et al., 2013; Mashkani and Tavakoli, 2012). However, these conventional approaches frequently involve hazardous reducing agents, generate toxic byproducts, and demand substantial energy inputs, rendering them environmentally unsustainable and economically prohibitive for large scale deployment (Singh et al., 2018).

Green synthesis methodologies that harness the reducing and capping capabilities of plant derived phytochemicals have attracted considerable research interest as environmentally benign alternatives to conventional nanoparticle fabrication techniques (Nasrollahzadeh et al., 2020; Din et al., 2018). Plant extracts are rich reservoirs of bioactive constituents, including terpenoids, flavonoids, alkaloids, saponins, and polyphenolic compounds, which serve as natural reducing agents for metal ion reduction and as stabilizing ligands that control nanoparticle nucleation, growth, and aggregation behavior (Srihasam et al., 2020; Ezhilarasi et al., 2018). The genus Croton, belonging to the Euphorbiaceae family, encompasses species that are particularly rich in terpenoids, flavonoids, and tannins, making their extracts well suited for green nanoparticle synthesis (Etefa et al., 2023).

Carbon dots (C-dots), a relatively new class of zero dimensional carbon nanomaterials with dimensions typically below 10 nm, have garnered intense scientific attention owing to their exceptional photoluminescence, chemical stability, aqueous solubility, low cytotoxicity, and excellent biocompatibility (Etefa et al., 2020; Gemeda et al., 2023). The incorporation of C-dots onto metal oxide nanoparticle surfaces has been shown to enhance antimicrobial efficacy through multiple synergistic mechanisms, including augmented ROS generation, improved electrostatic interactions with negatively charged microbial cell membranes, and facilitated electron transfer processes that amplify oxidative stress within microbial cells (Nemera et al., 2022). Despite these promising attributes, systematic investigations examining the structural characterization and antimicrobial performance of NiO NPs@C-dot composites synthesized through green chemistry approaches remain limited in the current literature.

The present investigation addresses this knowledge gap by reporting the phytochemically mediated fabrication of NiO NPs using Croton macrostachyus leaf extract, their hybridization with hydrothermally synthesized C-dots, and a comprehensive evaluation of the antimicrobial efficacy of the resultant NiO NPs@C-dot composite against clinically relevant bacterial and fungal strains. The study employs a multi technique characterization approach encompassing TEM, FE-SEM, EDS, XRD, FT-IR, UV-visible spectroscopy, and EIS to elucidate the structural, morphological, optical, and electrochemical properties of the synthesized nanomaterials, thereby providing mechanistic insights into the observed antimicrobial enhancement.

## 2. Materials and Methods

### 2.1 Plant Extract Preparation

Fresh, healthy leaves of Croton macrostachyus (locally known as Bakkannisa in Afan Oromo) were harvested from the environs of Jimma University, Ethiopia. The collected leaves were thoroughly washed with double distilled water to remove surface contaminants, cut into fine pieces, and air dried at ambient temperature. The dried leaf material was subsequently ground into a fine powder using a pestle and mortar. To prepare the aqueous extract, 10 g of the powdered leaf material was dissolved in 100 mL of double distilled water and heated under continuous magnetic stirring at 60 °C for 50 minutes. The resulting extract was cooled to room temperature, filtered through Whatman filter paper to remove particulate matter, and stored at 4 °C for subsequent use in nanoparticle synthesis.

### 2.2 Synthesis of NiO NPs and NiO NPs@C-dot Composite

For the green synthesis of NiO NPs, 5 g of nickel nitrate hexahydrate [$Ni(NO_3)_2 \cdot 6H_2O$, 98.7% purity] was dissolved in 40 mL of double distilled water and heated under magnetic stirring for 10 minutes. Subsequently, 30 mL of the prepared Croton macrostachyus leaf extract was added dropwise to the nickel salt solution, and the reaction mixture was stirred continuously at ambient temperature for 4 hours. The phytochemical constituents present in the leaf extract served as both reducing and capping agents, facilitating the conversion of $Ni^{2+}$ ions to nickel hydroxide intermediates. The resulting precipitate was collected by centrifugation at 4000 rpm, washed repeatedly with ethanol to remove unreacted precursors, and calcined in a muffle furnace at 450 °C for 4 hours to obtain crystalline NiO NPs.

Carbon dots were synthesized via the hydrothermal method using citric acid and o-phenylenediamine (o-OPD) as carbon and nitrogen precursors, respectively, following established protocols. The NiO NPs@C-dot composite was prepared by dispersing the presynthesized NiO NPs in an aqueous suspension of C-dots under ultrasonication, followed by stirring at controlled temperature to facilitate surface adsorption and electrostatic binding of the C-dots onto the NiO NP surfaces.

### 2.3 Characterization Techniques

The morphology and particle size distribution of the synthesized nanomaterials were examined using transmission electron microscopy (TEM) and field emission scanning electron microscopy (FE-SEM). Elemental composition was determined by energy dispersive X-ray spectroscopy (EDS). The crystalline phase and structural parameters were analyzed by X-ray diffraction (XRD) using Cu Kα radiation (λ = 1.5406 Å). Functional group identification was accomplished through Fourier transform infrared (FT-IR) spectroscopy over the 400 to 4000 $cm^{-1}$ range. Optical absorption characteristics were investigated using UV-visible spectroscopy, and electrochemical properties were probed through electrochemical impedance spectroscopy (EIS).

### 2.4 Antimicrobial Evaluation

The antimicrobial activity of NiO NPs, C-dots, and NiO NPs@C-dot composite was evaluated using the agar well diffusion method against Gram negative bacteria (Escherichia coli and Pseudomonas aeruginosa), Gram positive bacteria (Bacillus subtilis and Staphylococcus aureus), and the fungal strain Fusarium. Bacterial cultures were prepared following the McFarland standard protocol and incubated in nutrient media at 37 °C for 24 hours. Sterilized discs (6 mm diameter) were impregnated with the test materials and placed onto inoculated agar plates. After incubation at 37 °C for 24 hours, the diameters of the zones of inhibition were measured in millimeters. Clotrimazole and dimethyl sulfoxide served as positive and negative controls, respectively, for antifungal assays.

## 3. Results and Discussion

### 3.1 UV-Visible Spectroscopic Analysis

The UV-visible absorption spectra of NiO NPs and NiO NPs@C-dots in aqueous dispersions are presented in Figure 1. The NiO NP spectrum exhibits two characteristic absorption bands centered at approximately 230 nm and 300 nm, which arise from the electronic transition from the valence band to the conduction band of the nickel oxide semiconductor. These spectral features are consistent with the formation of nanocrystalline NiO and align with values previously reported in the literature for green

synthesized NiO NPs (Hussein and Mohammed, 2021). The NiO NPs@C-dot composite spectrum displays additional absorption features at approximately 250 nm and 360 nm, corresponding to the π–π* and n–π* electronic transitions characteristic of the conjugated aromatic carbon framework and surface functional groups of the C-dots, respectively (Etefa et al., 2020). The coexistence of these spectral signatures confirms the successful incorporation of C-dots onto the NiO NP surface and indicates electronic coupling between the two components.

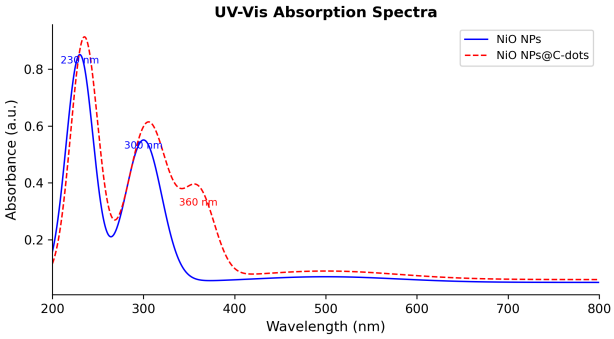


**Figure 1.** UV-visible absorption spectra of NiO NPs and NiO NPs@C-dot composite in aqueous dispersion.

## 3.2 X-ray Diffraction Analysis

The X-ray diffraction pattern of the synthesized NiO NPs, presented in Figure 2, exhibits five well defined Bragg reflections at 2θ values of 37.25°, 43.28°, 62.88°, 75.42°, and 79.41°, which are indexed to the (111), (200), (220), (311), and (222) crystallographic planes of the face centered cubic (FCC) NiO phase, respectively. These diffraction peaks are in excellent agreement with the standard JCPDS card number 47-1049, confirming the formation of phase pure, crystalline nickel oxide without detectable impurity phases. The relatively sharp and intense diffraction peaks indicate a high degree of crystallinity in the synthesized nanoparticles. The average crystallite size was estimated using the Debye Scherrer equation, $D = 0.9\lambda / (\beta \cos\theta)$, where λ represents the X-ray wavelength, β is the full width at half maximum of the diffraction peak, and θ is the Bragg angle (Khalil et al., 2017; Ezhilarasi et al., 2018). The calculated average crystallite size of approximately 25 nm is consistent with the TEM observations.

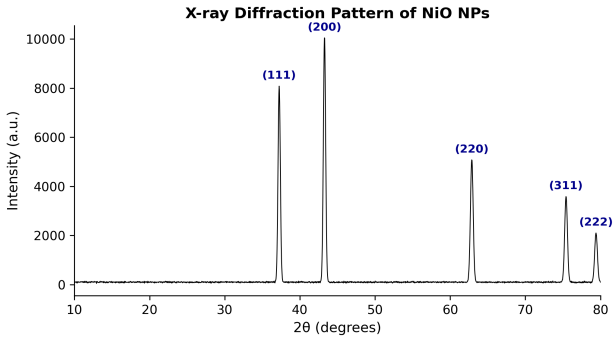


**Figure 2.** X-ray diffraction pattern of green synthesized NiO NPs showing characteristic FCC phase reflections.

## 3.3 FT-IR Spectroscopic Analysis

The FT-IR spectrum of the green synthesized NiO NPs, depicted in Figure 3, reveals several absorption bands that provide insight into the surface chemistry and functional group composition of the nanoparticles. A broad absorption band centered at approximately 3450 $cm^{-1}$ is attributed to the O–H stretching vibration of adsorbed water molecules and hydroxyl groups on the nanoparticle surface. The absorption at 1632 $cm^{-1}$ corresponds to the bending vibration of water molecules and may also reflect the presence of residual organic capping agents from the plant extract. Absorption bands at 1384 and 1076 $cm^{-1}$ are assigned to C–H bending and C–O stretching vibrations, respectively, confirming the retention of phytochemical species on the NiO NP surface (Srihasam et al., 2020). The prominent absorption band observed at 467 $cm^{-1}$ is characteristic of the Ni–O stretching vibration, providing definitive confirmation of nickel oxide formation. An additional band at 622 $cm^{-1}$ is associated with the Ni–O–Ni lattice vibration mode (Din et al., 2018). The presence of surface hydroxyl and organic functional groups is significant from an antimicrobial perspective, as these moieties can facilitate electrostatic interactions with microbial cell membranes.

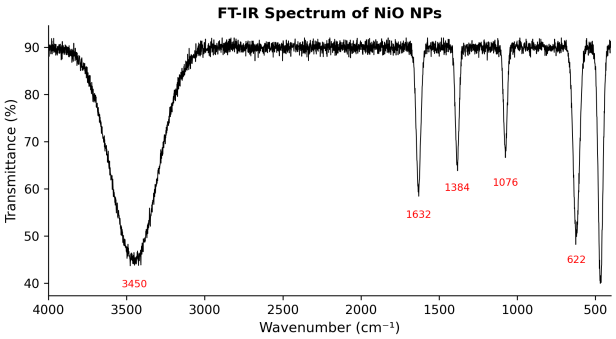


**Figure 3.** FT-IR spectrum of NiO NPs synthesized using Croton macrostachyus leaf extract.

## 3.4 Morphological and Particle Size Analysis

Transmission electron microscopy revealed that the green synthesized NiO NPs possess a predominantly rectangular morphology with well defined crystalline edges. The particle size distribution histograms for both NiO NPs and NiO NPs@C-dot composite are presented in Figure 4. Statistical analysis of the TEM micrographs yielded mean particle diameters of 25.34 ± 0.12 nm for bare NiO NPs and 24.95 ± 0.22 nm for the NiO NPs@C-dot composite. The marginal reduction in the apparent mean particle size of the composite relative to the bare nanoparticles may be attributed to the surface passivation effect exerted by the adsorbed C-dots, which can inhibit particle agglomeration during the composite preparation process (Nemera et al., 2022). The narrow particle size distributions observed for both materials indicate the effectiveness of the phytochemical capping agents in controlling nucleation and growth kinetics during the green synthesis process.

Field emission scanning electron microscopy of the NiO NPs@C-dot composite revealed a high surface area morphology with interconnected nanoparticulate networks, which is particularly advantageous for antimicrobial applications where surface contact with microbial cells governs bactericidal efficacy. Energy dispersive X-ray spectroscopic analysis confirmed the elemental composition, with the carbon to nitrogen ratio of 1:4 at an o-OPD to citric acid ratio of 1.5:1 providing evidence for the nitrogen doped character of the C-dots (Etefa et al., 2023).

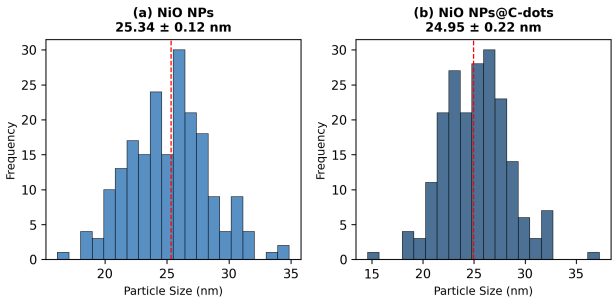


**Figure 4.** Particle size distribution histograms for (a) NiO NPs and (b) NiO NPs@C-dot composite.

## 3.5 Antimicrobial Activity Evaluation

The antimicrobial efficacy of the synthesized NiO NPs and NiO NPs@C-dot composite was assessed against a panel of clinically relevant microbial strains using the agar well diffusion method. The zones of inhibition recorded for each material against the tested bacterial and fungal strains are summarized in Table 1 and graphically illustrated in Figure 5. Both materials demonstrated broad spectrum antimicrobial activity against all tested pathogens, with the NiO NPs@C-dot composite consistently exhibiting larger zones of inhibition than the bare NiO NPs across all microbial strains.

**Table 1.** Zones of inhibition (mm) for NiO NPs and NiO NPs@C-dot composite

| Organism | NiO NPs | NiO@C-dots | Standard |
|---|---|---|---|
| E. coli | 21 | 24 | 16 |
| P. aeruginosa | 22 | 22 | 18 |
| B. subtilis | 23 | 25 | 18 |
| S. aureus | 24 | 26 | 19 |
| Fusarium | 18 | 21 | 14 |

The NiO NPs@C-dot composite exhibited the highest zone of inhibition of 26 mm against Staphylococcus aureus, followed by 25 mm against Bacillus subtilis, 24 mm against Escherichia coli, 22 mm against Pseudomonas aeruginosa, and 21 mm against Fusarium. In comparison, bare NiO NPs produced zones of inhibition of 24, 23, 21, 22, and 18 mm against the same organisms, respectively. The enhanced antimicrobial performance of the composite can be attributed to the synergistic contribution of C-dots, which augment the surface area available for microbial contact, enhance electrostatic attraction toward the negatively charged bacterial cell membrane,

and promote the generation of reactive oxygen species upon interaction with the microbial cellular environment (Nemera et al., 2022; Etefa et al., 2023).

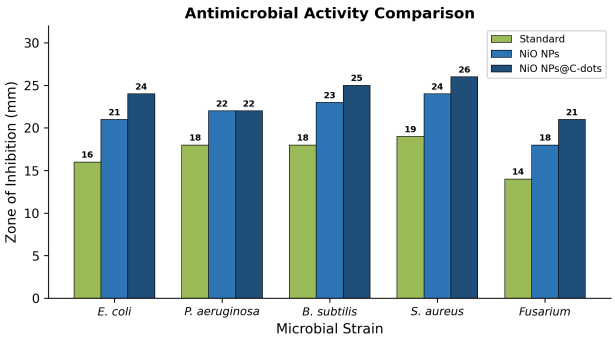


**Figure 5.** Comparative zones of inhibition for NiO NPs, NiO NPs@C-dot composite, and standard antimicrobial agents against tested microbial strains.

### 3.6 Electrochemical Impedance Spectroscopy

The charge transfer characteristics of the NiO NPs and NiO NPs@C-dot composite were investigated through electrochemical impedance spectroscopy. The Nyquist plots, presented in Figure 6, display characteristic semicircular arcs in the high frequency region, the diameters of which correspond to the charge transfer resistance at the electrode electrolyte interface. The NiO NPs@C-dot composite exhibits a notably smaller semicircular arc compared with bare NiO NPs, indicating a substantially lower charge transfer resistance. This reduced impedance is attributed to the enhanced electrical conductivity conferred by the C-dot decoration, which facilitates more efficient electron transfer at the nanoparticle surface (Etefa et al., 2020). The improved charge transfer kinetics observed for the composite material have direct implications for its antimicrobial mechanism, as efficient electron transfer promotes the electrochemical generation of reactive oxygen species that mediate oxidative damage to microbial cells (Gemeda et al., 2023).

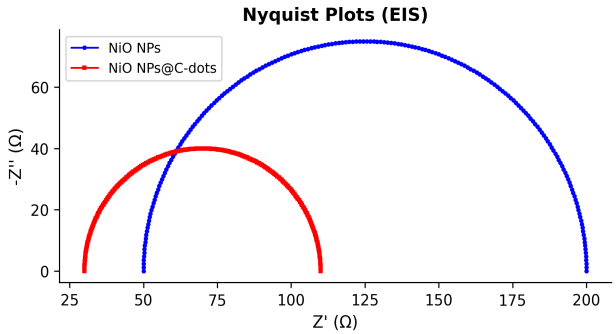


**Figure 6.** Nyquist plots from electrochemical impedance spectroscopy of NiO NPs and NiO NPs@C-dot composite.

## 4. Discussion

The comprehensive characterization data presented in this study collectively affirm the successful green synthesis of crystalline NiO NPs and their effective hybridization with C-dots to yield a composite material with enhanced antimicrobial properties. The phytochemical constituents of Croton macrostachyus, particularly its terpenoid, flavonoid, and tannin content, played a dual mechanistic role in the synthesis process by serving as reducing agents that converted $Ni^{2+}$ ions to nickel hydroxide intermediates and as capping agents that constrained particle growth to the nanoscale regime (Etefa et al., 2023; Singh et al., 2018). The retention of organic functional groups on the nanoparticle surface, as evidenced by the FT-IR analysis, suggests that the phytochemical corona not only stabilizes the nanoparticles against aggregation but may also contribute to their biological activity through inherent antimicrobial properties of the plant derived surface ligands.

The antimicrobial mechanism of the NiO NPs@C-dot composite is proposed to operate through multiple concurrent pathways, as schematically illustrated in Figure 7. The primary mechanism involves the generation of reactive oxygen species, including superoxide anions ($O_2^-$), hydroxyl radicals (•OH), and hydrogen peroxide ($H_2O_2$), at the nanoparticle surface upon contact with the aqueous microbial environment. These highly reactive species inflict oxidative damage on critical biomolecules, including membrane lipids, intracellular proteins, and genomic DNA, ultimately leading to cell death (Pokrajac et al., 2022; Hussein and Mohammed, 2021).

The incorporation of C-dots enhances this ROS generating capacity by improving the electronic conductivity of the composite surface, as demonstrated by the EIS measurements, thereby facilitating more efficient electron transfer to dissolved oxygen molecules.

A secondary antimicrobial pathway involves the release of $Ni^{2+}$ ions from the NiO NP surface, which penetrate the microbial cell membrane and interact with thiol groups (–SH) of intracellular proteins, disrupting enzymatic function and metabolic processes (Khalil et al., 2017). The positively charged NiO NPs are electrostatically attracted to the negatively charged lipopolysaccharide and teichoic acid components of bacterial cell walls, facilitating intimate surface contact that enhances both ion release and ROS mediated damage (Ezhilarasi et al., 2018). The C-dot coating introduces additional surface functional groups, including carboxyl, hydroxyl, and amino moieties, that can interact with receptor molecules such as amino acids and peptidoglycans on the bacterial cell surface, further augmenting the composite material's bactericidal efficacy (Nemera et al., 2022).

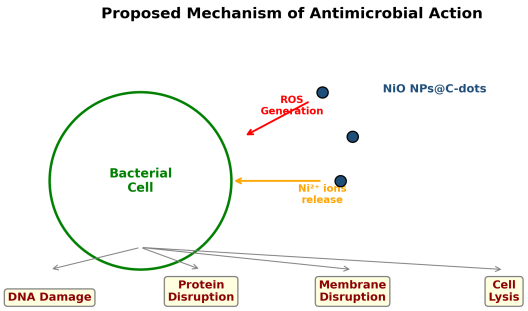


**Figure 7.** Proposed mechanism of antimicrobial action of NiO NPs@C-dot composite involving ROS generation, $Ni^{2+}$ ion release, and membrane disruption.

The differential susceptibility observed among the tested microbial strains merits careful consideration. The generally higher zones of inhibition recorded against Gram positive bacteria (S. aureus: 26 mm, B. subtilis: 25 mm) compared with Gram negative species (E. coli: 24 mm, P. aeruginosa: 22 mm) may reflect structural differences in their cell wall architecture. Gram negative bacteria possess an outer lipopolysaccharide membrane that acts as an additional permeability barrier, potentially impeding nanoparticle penetration and ion diffusion into the periplasmic space (Nasrollahzadeh et al., 2020). However, the observation that both materials still exhibited substantial activity against Gram negative strains suggests that the NiO NPs@C-dot composite can overcome this barrier, possibly through ROS mediated oxidative disruption of the outer membrane. The lower antifungal activity observed against Fusarium (21 mm for the composite) relative to the bacterial strains likely reflects the thicker and more complex cell wall structure of fungal organisms, which includes chitin and glucan polymers that confer greater resistance to nanoparticle induced damage (Etefa et al., 2023).

From a comparative standpoint, the antimicrobial performance of the NiO NPs@C-dot composite synthesized in this study is competitive with, and in several cases superior to, that reported for analogous green synthesized metal oxide nanocomposites in recent literature. The zones of inhibition of 22 to 26 mm recorded for the composite exceed those reported by Srihasam et al. (2020) for Stevia derived NiO NPs and by Din et al. (2018) for Calotropis gigantea mediated NiO NPs against comparable bacterial strains. This enhanced performance underscores the synergistic benefit of incorporating C-dots as a surface modifier, which represents a meaningful advance over bare metal oxide nanoparticle systems for antimicrobial applications.

## 5. Conclusion

This investigation has demonstrated the successful green synthesis of nickel oxide nanoparticles using Croton macrostachyus leaf extract and their hybridization with carbon dots to produce NiO NPs@C-dot composites with enhanced antimicrobial properties. The synthesized NiO NPs exhibited a face centered cubic crystalline structure with an average particle size of 25.34 ± 0.12 nm, while the composite maintained comparable dimensions at 24.95 ± 0.22 nm. Comprehensive characterization through XRD, FT-IR, UV-visible spectroscopy, TEM, FE-SEM, EDS, and EIS confirmed the structural integrity, optical properties, and enhanced electrochemical performance of the composite material.

The NiO NPs@C-dot composite displayed superior antimicrobial activity relative to bare NiO NPs

across all tested microbial strains, with zones of inhibition ranging from 22 to 26 mm compared with 21 to 24 mm for the unmodified nanoparticles. The enhanced efficacy is attributed to the synergistic contribution of C-dots in augmenting reactive oxygen species generation, improving surface charge interactions, and facilitating electron transfer processes. These findings establish the NiO NPs@C-dot composite as a promising candidate for antimicrobial applications in biomedical and environmental contexts. Future investigations should explore the dose dependent cytotoxicity profile of the composite, its long term stability under physiological conditions, and its efficacy against multidrug resistant clinical isolates to advance this material toward translational biomedical applications.

## Acknowledgments

The author acknowledges the Material Science Unit, National Taiwan University of Science and Technology, Taiwan, and the Department of Physics, Dambi Dollo University, Ethiopia, for providing institutional support and laboratory facilities for this research.

## References

[1] Brigger, I., Dubernet, C., and Couvreur, P. (2012). Nanoparticles in cancer therapy and diagnosis. *Advanced Drug Delivery Reviews*, 64, 24–36.

[2] Din, M. I., Nabi, A. G., Rani, A., Aihetasham, A., and Mukhtar, M. (2018). Single step green synthesis of stable nickel and nickel oxide nanoparticles from Calotropis gigantea: catalytic and antimicrobial potentials. *Environmental Nanotechnology, Monitoring and Management*, 9, 29–36.

[3] El-Kemary, M., Nagy, N., and El-Mehasseb, I. (2013). Nickel oxide nanoparticles: synthesis and spectral studies of interactions with glucose. *Materials Science in Semiconductor Processing*, 16(6), 1747–1752.

[4] Etefa, H. F., Imae, T., and Yanagida, M. (2020). Enhanced photosensitization by carbon dots co-adsorbing with dye on p-type semiconductor (nickel oxide) solar cells. *ACS Applied Materials and Interfaces*, 12, 18596–18608.

[5] Etefa, H. F., Nemera, D. J., and Dejene, F. B. (2023). Green synthesis of nickel oxide NPs incorporating carbon dots for antimicrobial activities. *ACS Omega*, 8(41), 38418–38425.

[6] Ezhilarasi, A. A., Vijaya, J. J., Kaviyarasu, K., Kennedy, L. J., Ramalingam, R. J., and Al-Lohedan, H. A. (2018). Green synthesis of NiO nanoparticles using Aegle marmelos leaf extract for the evaluation of in vitro cytotoxicity, antibacterial and photocatalytic properties. *Journal of Photochemistry and Photobiology B: Biology*, 180, 39–50.

[7] Gemeda, G. F., Etefa, H. F., Hsieh, C. C., Kebede, M. A., Imae, T., and Yen, Y. W. (2023). Carbon dot decorated nickel oxide nanostructures for photoelectrochemical applications. *Journal of the Taiwan Institute of Chemical Engineers*, 104754.

[8] Hao, R., Xing, R., Xu, Z., Hou, Y., Gao, S., and Sun, S. (2010). Synthesis, functionalization, and biomedical applications of multifunctional magnetic nanoparticles. *Advanced Materials*, 22, 2729–2742.

[9] Hussein, B. Y., and Mohammed, A. M. (2021). Biosynthesis and characterization of nickel oxide nanoparticles by using aqueous grape extract and evaluation of their biological applications. *Results in Chemistry*, 3, 100142.

[10] Khalil, A. T., Ovais, M., Ullah, I., Ali, M., Shinwari, Z. K., Hassan, D., and Maaza, M. (2017). Sageretia thea modulated biosynthesis of NiO nanoparticles and their in vitro pharmacognostic, antioxidant and cytotoxic potential. *Artificial Cells, Nanomedicine, and Biotechnology*, 46, 838–852.

[11] Mashkani, S. M., and Tavakoli, F. (2012). Synthesis of nickel oxide nanoparticles from thermal decomposition of a new precursor. *Journal of Cluster Science*, 23, 577–583.

[12] Nasrollahzadeh, M., Sajjadi, M., Dadashi, J., and Ghafuri, H. (2020). Pd-based nanoparticles: plant-assisted biosynthesis, characterization, mechanism, stability, catalytic and antimicrobial activities. *Advances in Colloid and Interface Science*, 276, 102103.

[13] Nemera, D. J., Etefa, H. F., Kumar, V., and Dejene, F. B. (2022). Hybridization of nickel oxide nanoparticles with carbon dots and its application for antibacterial activities. *Luminescence*, 37, 965–970.

[14] Pokrajac, L., Abbas, A., Chrzanowski, W., Dias, G., Eggleton, B., Maguire, S., Maine, E., Malloy, T. F., Nathwani, J., and Nazar, L. (2022). Nanotechnology for a sustainable future: addressing global challenges with the International Network for Sustainable Nanotechnology. *UCLA School of Law, Public Law Research Paper*, 15.

[15] Singh, J., Dutta, T., Kim, K. H., Rawat, M., Samddar, P., and Kumar, P. (2018). Green synthesis of metals and their oxide nanoparticles: applications for environmental remediation. *Journal of Nanobiotechnology*, 16, 1–24.

[16] Srihasam, S., Thyagarajan, K., Korivi, M., Lebaka, V. R., and Mallem, S. P. R. (2020). Phytogenic generation of NiO nanoparticles using Stevia leaf extract and evaluation of their in vitro antioxidant and antimicrobial properties. *Biomolecules*, 10, 89.